7th ECCOMAS Thematic Conference on Smart Structures and Materials
SMART 2015
A.L. Araújo, C.A. Mota Soares, et al. (Editors)

Active structural acoustic control of gear-box systems using a pair of piezo-based rotating inertial actuators

G. Zhao[*], N.Alujevic[*], B. Depraetere[†], P.Sas[*],

[*] KU Leuven,
Production Engineering, Machine Design and Automation (PMA) Section
Celestijnenlaan 300b - box 2420
3001 Heverlee, Belgium
guoying.zhao@kuleuven.be
neven.alujevic@kuleuven.be
paul.sas@kuleuven.be

[†] FMTC, division of Flanders Make
Celestijnenlaan 300d - box 4027
3001 Heverlee, Belgium
bruno.depraetere@fmtc.be

Key words: Piezoelectric element, rotating inertial actuator, FxLMS, active structural acoustic control

Summary: *In this paper, two Piezo-Based Rotating Inertial Actuators (PBRIAs) are considered for the suppression of the structure-borne noise radiated from gearbox systems. As add-on devices, they can be directly mounted on a rotational shaft, in order to intervene as early as possible in the transfer path between disturbance source and the noise radiators. A feedforward control strategy similar to the FxLMS control algorithm is proposed to generate the appropriate actuation signals. Since the add-on devices rotate along with the shaft, the strategy aims to limit the influence of the secondary plant variation over the course of the shaft revolution on the control performance. The proposed active vibration control approach is tested on an experimental test bed comprising a rotating shaft mounted in a frame to which a noise-radiating plate is attached. The disturbance force is introduced by an electrodynamic shaker. The experimental results show that when the shaft rotates below 180 rpm, more than a 15 dB reduction can be achieved in terms of plate vibrations, along with a reduction in the same order of magnitude in terms of noise radiation.*

1 INTRODUCTION

Gearboxes are commonly found in mechanical power transmission systems such as automotive, aerospace, and industrial applications. In these applications, dynamic forces are induced as a result of the gear teeth profile errors and time varying stiffness during the gearmeshing. The induced force creates unwanted vibrations on the rotating shaft, which then transmit through the bearings to the housing, where the resulting vibrational power is eventually converted into noise. In order to reduce the noise level, techniques such as sound absorption based insulation including encapsulation can be used to interrupt the airborne sound transmission from the systems to the environment. These passive sound control

techniques are typically used to deal with noise at higher frequencies. At lower frequencies, where the acoustic wavelength is much larger than the maximum permissible thickness of the insulation layers, active noise control strategies can be considered instead [1]-[4]. These however become more complicated and more expensive, or alternatively less efficient, if the size of the enclosure where the sound is controlled [3] is comparatively large. Many error sensors (microphones) and control actuators (loudspeakers) are necessary for good control performance since their required number increases with the size of the room. An alternative is using force actuators to achieve noise reduction, this is known as active structural acoustic control (ASAC) and can be done by applying control forces on the surfaces [5], [6], [11]-[17] or by isolating the transmission forces from the radiating surfaces [18]-[25]. In case forces are applied directly to the noise radiation surfaces, passive tuned mass dampers [7]-[10], inertial shakers [11]-[13], reactive actuators [14] or piezoelectric patches [15]-[17] are often employed to produce the control forces. However, this approach may become cumbersome and expensive for large and complex systems which have many radiating surfaces.

On the other hand, in the active vibration isolation approach it is attempted to waken the transmitted vibrations in the structural transfer paths before they reach the noise radiating surfaces. This may yield a control system that is less complex in case there is a limited number of well-defined vibration transmission paths. With gearboxes paths typically include in bearings that support revolving shafts. Several studies based on this approach have been published recently. Rebbechi et al. [19] proposed to integrate two pairs of magnetostrictive actuators into a double row bearing, which is mounted on the input shaft next to the input pinion, with the aim of actively isolating the vibration transmitted from the shaft to the housing. A reduction of 20-28 dB can be obtained in the housing vibration at the fundamental gear mesh frequency. Pinte et al. and Stallaert et al. [20]-[21] adopted a similar approach, but used two piezoelectric actuators instead, which are perpendicularly mounted onto one of the support bearing locations in order to limit the force transmitted from the shaft to the housing. Instead of placing the actuator in series with the original bearing, Guan et al. [22] and Li et al. [23] proposed to mount the control actuator in parallel, directly on the shaft via an additional bearing (active shaft transverse vibration control). In such a case, the system suspension stiffness is not influenced by the introduction of the actuator. Chen and Brennan [24] investigated an inertial actuator control concept where three magnetostrictive inertial shakers are positioned tangentially at 120˚ intervals on the gear body, in order to suppress the gear vibrations at the source. The above mentioned actuation concepts for the suppression of gearbox housing vibrations are theoretically compared by Guan et al. [25]. In this theoretical study, the actuation effort, control robustness and implementation costs are taken into account as the comparison criteria for four different actuation concepts. The shaft transverse vibration active control approach appeared to be the best compromise regarding the required amplitude of the control force below 500 Hz while also yielding a reasonable control robustness and a limited implementation cost.

In this study, an axisymmetric piezo-based rotational inertial actuator, which can be installed directly on the rotating shaft as an add-on device, is proposed and studied experimentally. The benefit of this add-on approach is that the machine stiffness is not affected as is the case with for example active bearings. Another advantage is the relative ease of implementation in a practical setting as no major structural modification is required. Furthermore, the active element is not in a critical path of the machine such that a possible failure of the piezoelectric element does not necessarily affect the functionality of the machine.

One of the aims of this paper is to investigate if it is feasible to suppress tonal structural

borne noise/vibration of gearbox systems using the co-rotating actuator-stationary sensor concept. The employed control algorithm is similar to the filtered reference least mean squares (FxLMS) algorithm [1]-[2]. The difference however lies in the fact that the secondary plant is strongly time-varying with a complete permutation of its amplitude and phase within one revolution of the shaft. Thus in the present study the inverse of the secondary plant model is used which is placed between the controller output and the error sensor, whereas in the standard FxLMS control scheme, the model of the secondary plant is typically placed between the reference signal and the input of the controller. By using the proposed algorithm, the time varying secondary plant effect can be eliminated such that the variation of the controller coefficients can be bounded in a limited range, which would not the case for the standard FxLMS controller.

This paper is organized as follows. The design of the piezo based rotating inertial actuator (PBRIA) is briefly covered in Section 2, along with the experimental test bed used to evaluate its performance. The implementation of the proposed control algorithm is discussed, in Section 3, followed by a presentation of the achieved results in Sections 4.

2 GENERAL SPECIFICATIONS

Figure 1 shows the developed prototype of the piezo-based rotating inertial actuator. The idea behind the design of the PBRIA is to use a piezoelectric actuator to introduce a force between a rotating element (e.g. the shaft) and a ring-shaped mass rotating together with the shaft. By accelerating the ring-shaped mass, compensating forces can be generated on the shaft. A Piezomechanik HPSt 150/20 piezoelectric stack actuator is used. Although the developed PBRIA has sufficient force capacity to compensate the disturbances on the test bed in the frequency range of interest (200 Hz to 1000 Hz), in industrial applications, where excitation forces are larger, longer piezoelectric actuators or heavier proof masses should be used to generate the required compensating force.

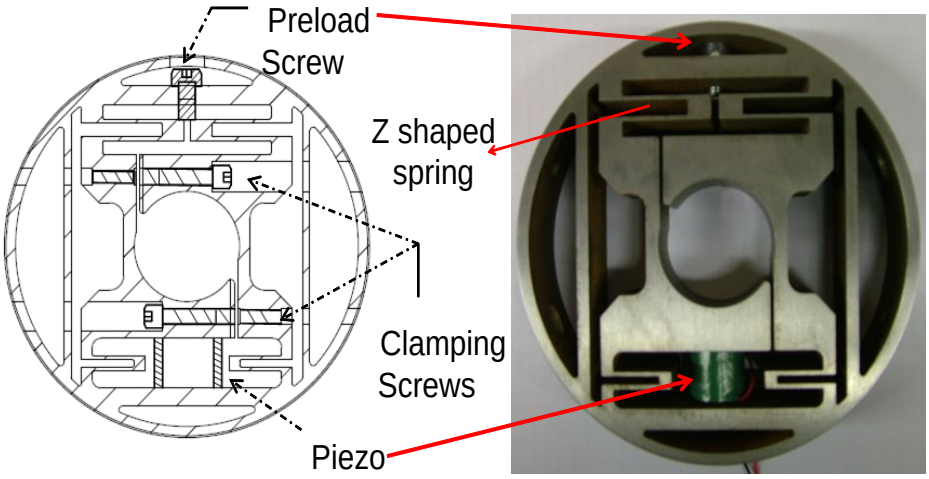

Figure 1: The developed piezo-based rotating inertial actuator

In order to eliminate the need for an additional fixture mechanism, the inner collar, as shown in Figure 1, is split. Moreover, the splits are offset in order to prevent stress concentration on the piezoelectric actuator. Note that the maximum applicable negative voltage for the piezoelectric stack actuator is much smaller than the maximum applicable positive voltage so that the piezoelectric stack actuator cannot withstand a high level of tension force. In practice, this issue can be solved by applying a preload force to the

piezoelectric actuator. In this design, the piezoelectric actuator is preloaded by pre-stressing two Z shaped springs on the opposite side, such that it is capable of applying push/pull forces. A cap screw is then used to tighten the Z shaped springs and a pre-stress of approximately 250 N is applied to the piezoelectric element.

The proof mass (outer ring) of the PBRIA is suspended by four Z shaped springs. These springs are designed to realise a low translational stiffness in one radial direction (vertical direction in Fig. 1) while guaranteeing a high stiffness in the tangential direction (horizontal direction in Fig. 1) as well as a high torsional stiffness. The high torsional stiffness is required in order to avoid excessive bending stress for the piezoelectric actuator in the low frequency range.

A representative set-up for gearbox systems is constructed in order to demonstrate the feasibility of the proposed active structural acoustic control (ASAC) control approach, which is shown in Figure 2. The test bed consists of a shaft which is mounted in a frame by a cylindrical bearing at one side and a double angular contact ball bearing at the other side. This latter bearing is mounted in a ring-shaped module in which two piezoelectric sensors are installed to measure the transmitted forces between the shaft and the frame. Close to this bearing, two PBRIAs are perpendicularly mounted on the shaft such that control forces can be generated in all directions while the shaft rotates. An electric motor is connected to the shaft to drive the shaft. A metal plate with dimensions of $40\text{mm} \times 30\text{mm} \times 2\text{mm}$ (length × height × width) is connected to the frame using two square beam profiles and acts as a noise radiator. The dimensions of the different parts are chosen such that the test bed has a dynamic and acoustic behavior representative for gearboxes [21]. A slip ring is mounted on the shaft close to the PBRIAs to provide electrical connections to the non-rotating controller.

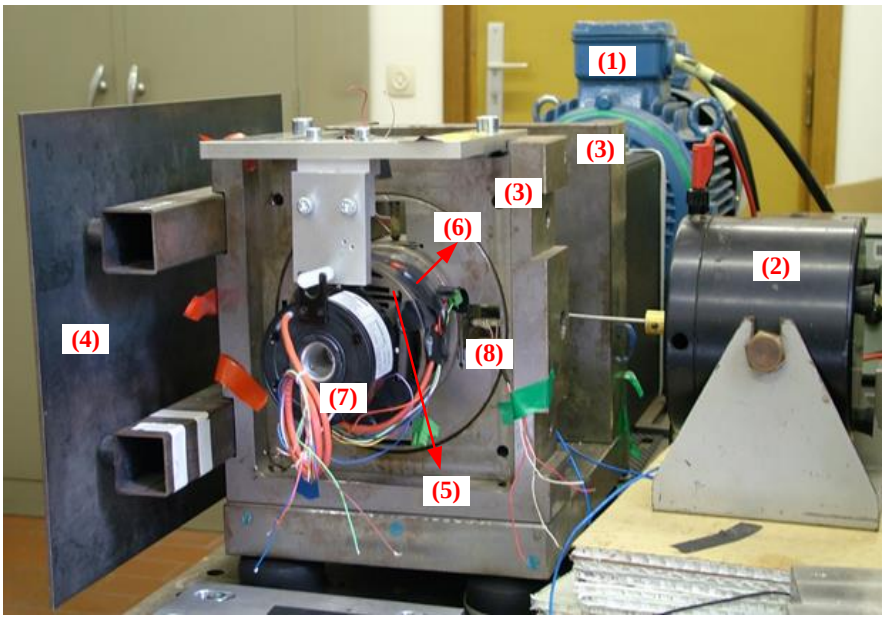

Figure 2: The experimental set-up of the test bed: (1) Motor; (2) Disturbance shaker; (3) Frame; (4) Noise radiating plate; (5) PBRIA 1; (6) PBRIA 2; (7) Slip ring; (8) Force sensor.

The disturbance force is generated by an electrodynamic shaker which is connected to the shaft via an additional bearing. With the additional bearing, it is possible to introduce arbitrary disturbance forces on the rotating shaft as such it is possible to simulate gear mesh forces.

A number of sensors are installed on and around the test bed so as to measure the performance of the proposed control approach. The layout of the sensor configuration is shown in Figure 3, where two accelerometers are used to measure the structural vibrations, one microphone is used to register the noise level in front of the plate at a distance of approximately 30 cm, and one force gauge, placed between the bearing close to the PBRIA and the frame, is used to record the transmitted force. One of the accelerometers is placed on the frame to measure vibrations in the x and y axes, while the other one is mounted in the center of the noise radiating plate to measure the vibrations normal to the plate, this signal will serve as the error signal for the active controller in the experiments of this study.

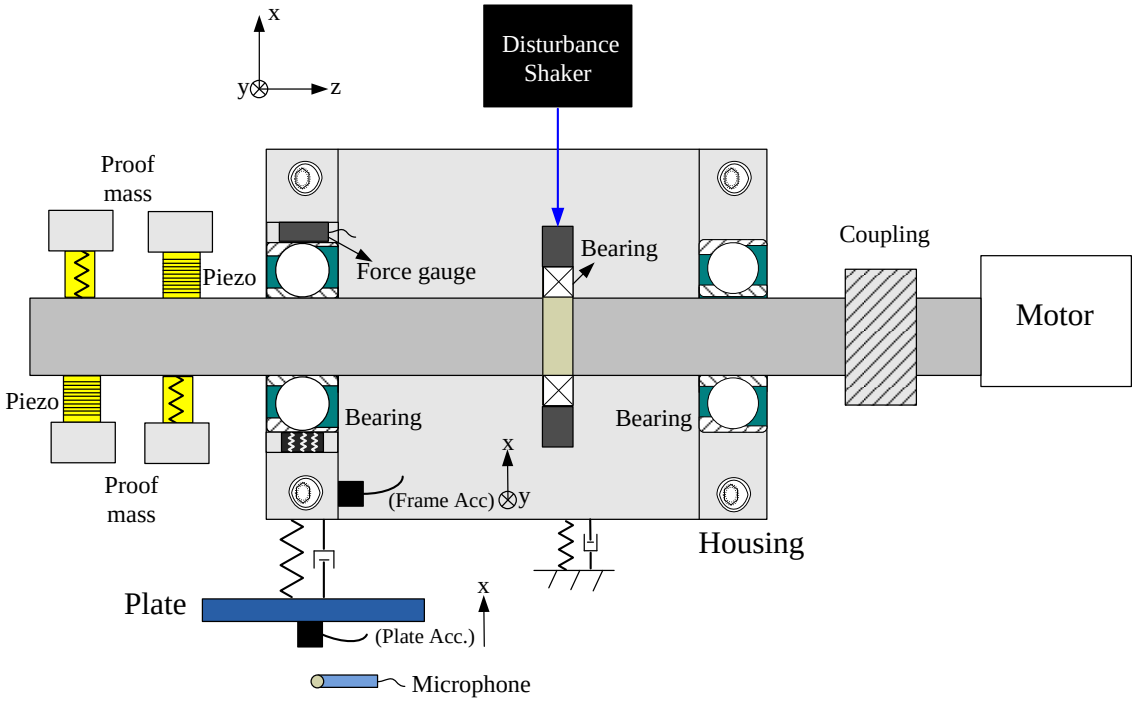

Figure 3: A cross-sectional view of the experimental set-up

3 CONTROL ALGORITHM

In this section, the proposed control algorithm, which is a feedforward control approach similar to the FxLMS control algorithm, is introduced. In the first part, the FxLMS control algorithm is briefly reviewed and a general form of the proposed control algorithm is presented. The review of the FxLMS controller is done in order to enable a straightforward interpretation of the principles behind the proposed algorithm. The second part of this section deals with the modification of the algorithm to a Single Input Multi Output (SIMO) setting for controlling two PBRIAs with time varying secondary plants.

Figure 4 (a) shows the block diagram of the FxLMS control algorithm. The core of the control scheme is an adaptive digital filter, which is usually implemented by a finite impulse response filter (FIR), denoted as $W(k)$. The coefficients of $W(k)$ are updated so that the expected mean square error (MSE) of a chosen error signal $e(k)$, $E\left[e^2(k)\right]$ is minimized. This is usually done by using the steepest decent method. Using the instant squared error signal $e^2(k)$ to estimate the MSE, the well-known least mean square (LMS) algorithm for updating the coefficients of is derived:

$$W(k+1) = \beta W(k) + \mu r(k) e(k) \tag{1}$$

where μ is the convergence coefficient, β is the power constraint with $0 < \beta \leq 1$, $e(k)$ is the instantaneous error, i.e., the difference between the disturbance signal $d(k)$ and the secondary plant ($S(q)$) output $y(k)$, and $r(k)$ is the filtered reference signal which is the convolution of the reference $x(k)$ and the estimated secondary plant $\bar{S}(q)$. Generally, the parameter μ should be as large as possible without compromising the stability of the system. A suitable value of control effort constraint β should be introduced to limit the output power to avoid nonlinear distortion [2]. If the parameter β is set to a value other than unit, the FxLMS algorithm becomes the leaky FxLMS algorithm.

For the conventional FxLMS control algorithm, its performance is highly determined by the dynamic properties of the secondary plant and the disturbance signal. If the secondary plant is time-variant, convergence to the optimal settings is difficult and leads to a poor performance or instability especially when the rate of the change is fast. In that case, it is desirable that the change of the dynamics of the secondary plant can be compensated such that the variation of the controller coefficients is limited; and the control performance is improved. To this end, a modified version of the FxLMS algorithm is proposed. Its control scheme is shown in Figure 4 (b), where $\left[\bar{S}(q)\right]^{-1}$ is the estimate of the inverse of the secondary plant and all the other variables have the same meanings as that shown in Figure 4 (a). In this case, the driving signal to the actuator is $u'(k)$, which is the convolution of the output signal of the controller $u(k)$ and the filter $\left[\bar{S}(q)\right]^{-1}$. If a perfect inverse model is derived, the modified FxLMS algorithm will behave like a standard LMS control algorithm, which is unaffected by the dynamics of the secondary plant and thus outperforms the FxLMS controller counterpart when the secondary plant is time varying.

Depending on the availability of the reference signal, the proposed algorithm can be used to control both broadband and narrowband disturbances. For the gearbox systems, the vibration and acoustic response is dominated by tonal peaks that occur at the fundamental gear meshing frequency and its harmonics. As such, this study mainly focuses on suppressing tonal disturbances and thereby the periodic version of the algorithm is implemented and a sinusoidal signal of the same frequency as the disturbance is used as the reference signal. Since two PBRIAs are used in the experiments, a SIMO form of the proposed algorithm is investigated. In this SIMO system, the two outputs refer to the driving signals for the two PBRIAs and the input refers to the error signal used to update the controller coefficients. In experiments, the secondary plants are between the driving signals for the two PBRIAs and the accelerometer output signal on the radiated plate. As mentioned earlier, the chosen error sensor is mounted on the fixed parts of the test bed whereas the piezoelectric actuators are rotating together with the shaft. This means that the constructed secondary plants are continuously changing with respect to the shaft angular position, implying that the secondary plants are time varying as well as their inversions.

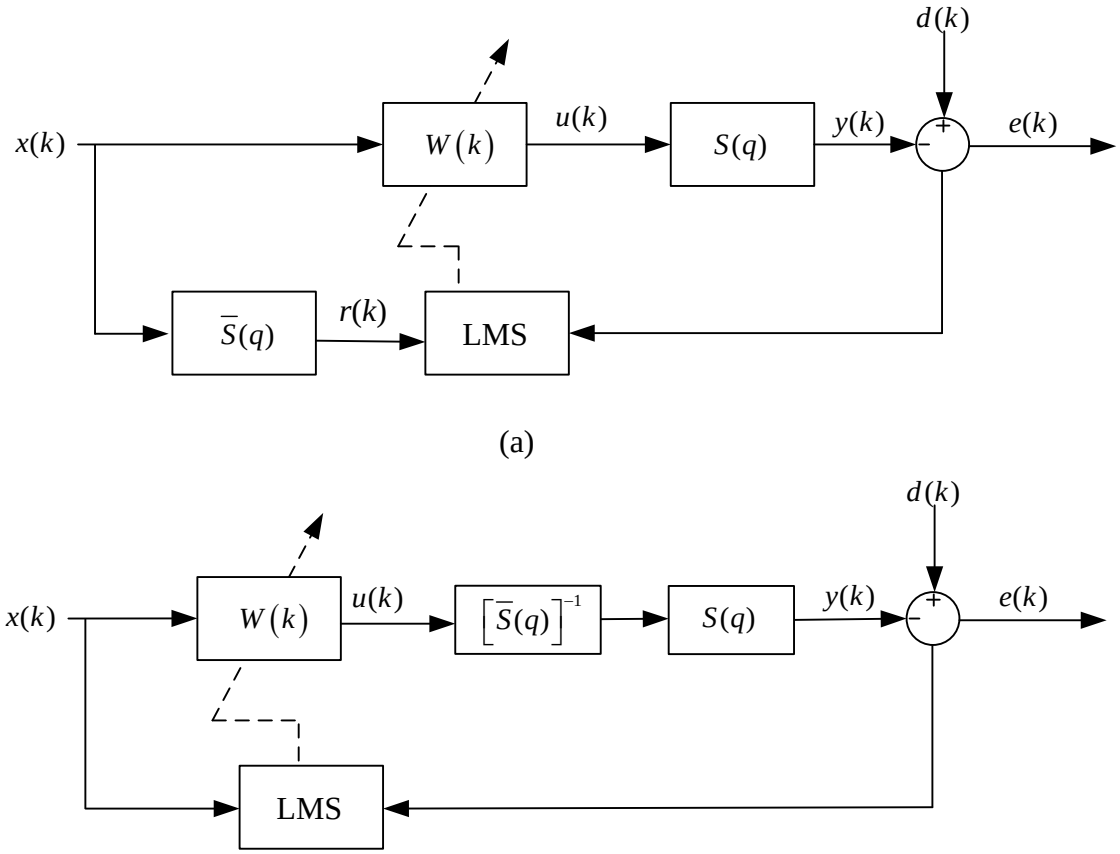

Figure 4: The block diagram of (a) the FxLMS algorithm and (b) the proposed algorithm

Two practical issues arise when it comes to the design of $\left[\bar{S}(q)\right]^{-1}$. Firstly and most importantly, it is challenging to derive an efficient model for a time varying system without sufficient prior knowledge, especially when the system is complicated, such as for the system that is considered in this paper. An often used solution to this problem is based on interpolation, where the system can be approximated by interpolating some local linear models. In this paper, the idea is to fix the system at several angular positions and then approximate the plant locally for each position, after which the overall plant model is obtained by linearly interpolating between the two most adjacent estimated plants. The second issue is related to the inverse of the system model, where stability and causality problems need to be addressed when an IIR control filter is employed. Since in this paper, a FIR filter is used to model the secondary plant at the considered sinusoidal disturbance the instability caused by the inverse is no issue.

Finally, the block diagram of the overall proposed control algorithm is shown in Figure 5, where various symbols have the following meanings: $x(k)$ represents the reference signal, the disturbance is presented by $d(k)$; $W(k)$ is an 2nd order adaptive FIR filter; $u(k)$ is the output signal of the control filter, which passes through the two inverse models of the secondary plants $\left[\bar{S}_1(q)\right]_\theta^{-1}$ and $\left[\bar{S}_2(q)\right]_\theta^{-1}$ generating two driving signals $u_1'(k)$ and $u_2'(k)$

for the piezo-actuators respectively; $e(k)$ is the error signal measuring the plate vibrations. The cost function for updating the controller coefficients is the squared error signal $e(k)$.

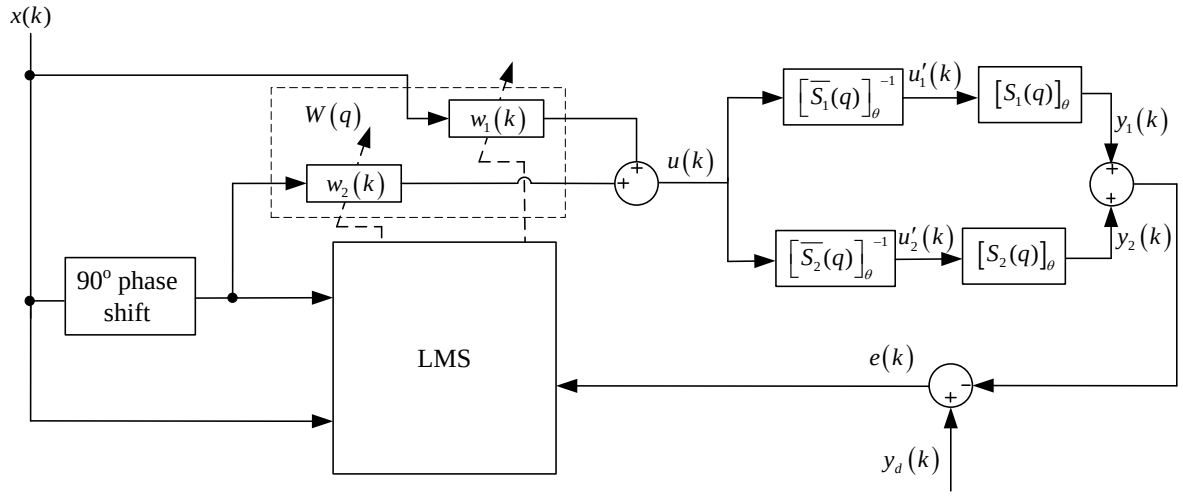

Figure 5: The flowchart of the SIMO form of the proposed algorithm utilizing a pair of orthogonal harmonic reference signals

4 EXPERIMENTAL VALIDATION

The purpose of the experiments in this section is to examine the performance of actively controlled PBRIAs in the test bed presented in Section 2. Prior to describing the results obtained, some system parameters are defined first.

A dSpace DS 1006 system has been used for control purposes and for data acquisition. To implement the controllers, a MATLAB Simulink model is developed and then downloaded to its processor unit. The same dSpace system also has several digital analog convertors and analog digital convertors to drive and receive signals to and from the actuators and sensors. All these signals originating from and fed into the dSpace system are filtered by an external low pass filter with a 1 kHz cut-off frequency. The adaptive controller is updated at a sampling frequency of 20 kHz, but the measured data are recorded at a frequency of 2.5 kHz in order to reduce the memory usage for storing of the data. An encoder with a resolution of 1024 pulses per revolution is utilized to measure the rotational position of the shaft, the signals from which are then processed by the dSpace control broad 3001 to calculate the instant angular position.

As described earlier, the horizontally measured acceleration of the plate is taken as the error signal. The disturbance is provided by the electrodynamic shaker, as shown in Figure 3, which is driven with a sinusoidal signal at 371 Hz throughout the study. This frequency corresponds to one of the resonances of the sound radiating plate. The sine wave sent to this shaker is directly taken as the reference signal for the proposed algorithm in the Simulink model. Thus, a perfect correlation between the reference and the disturbance is assumed. In real-life applications, a tachometer signal, which provides information concerning the disturbance frequency, can be taken as the reference signal. This signal can be acquired for example from an optical sensor measuring the rotational motor speed. In order to assure an adequate level of coherence between the reference and disturbance signals, the measured pulse train can be fed into a frequency estimator to estimate the instant rotating speed [22].

4.1 Secondary plant identification and its inversion

The procedure to design the inverted secondary plants consists of three steps, which can be summarized as follows:

- Define the frequency range where disturbance rejection is required.
- Identify the physical secondary plant statically such that the inverse model for that position can be derived based on the identified model.
- Repeat the second step for multiple angles, so that an interpolation scheme can be added to obtain a time varying inverted secondary plant.

In the first step, it is decided in which frequency range the controller should be active. This depends on the frequency content of the disturbance to be cancelled. In this paper, only a single frequency is considered, which also means that an FIR filter with only 2 coefficients is sufficient to model the dynamics of the secondary plant at a single angular position.

For the second step, the coefficients of the FIR filter for modelling the secondary plant can be determined off-line with an LMS adaptive algorithm [2]. The process consists of exciting the secondary path with a sine wave and simultaneously providing the same signal as the reference to a conventional LMS algorithm. After the convergence of the algorithm, the controller coefficients will then resemble the secondary path impulse response. Afterwards, the inverse plant can also be modelled as a 2nd order FIR filter. The relationship between the original 2nd order FIR filter $P=\begin{bmatrix} a & b \end{bmatrix}$ and its inversion $P'=\begin{bmatrix} c & d \end{bmatrix}$ can be determined based on the principles of opposite phase and reciprocal of the amplitude:

$$c=-\sqrt{\left(-4a^2b^2\left(\sin(\theta)\right)^2+4\cos(\theta)a^3b+4ab^3\cos(\theta)+a^4+6a^2b^2+b^4\right)^{-1}}\left(2b\cos(\theta)+a\right) \tag{2}$$

$$d=\sqrt{\left(-4a^2b^2\left(\sin(\theta)\right)^2+4\cos(\theta)a^3b+4ab^3\cos(\theta)+a^4+6a^2b^2+b^4\right)^{-1}}b \tag{3}$$

In the third step, the goal is to obtain an extended model that is valid for all angular positions. This is needed since, as mentioned above, the secondary plants are angular position dependent. In this step, we therefore identify the secondary plant at 32 angular positions in one revolution with an interval of 11.25°. The 0° position is defined when the piezoelectric actuator of PBRIA 1, as shown in Figure 2, is parallel to the disturbance. Once the 32 models are identified, the inverse of all models can be derived by using Eq. (2) and (3).

Figure 6 (a) and (b) show the amplitude and phase of the secondary plant and the inverted secondary plant between the voltage to the piezoelectric actuator in PBRIA 1 and the measured plate vibrations at 371 Hz, while Figure 6 (c) and (d) present the amplitude and phase of the FRFs between the voltage to the piezoelectric actuator in those for PBRIA 2. As can be seen, the FRFs of the two secondary plants vary with respect to the angular positions, where the crests and troughs of the curves are located at these positions when the actuation direction of the PBRIA is parallel and perpendicular to the direction of the sensors. For the derived inverted secondary plant models, the corresponding FRFs show an opposite phase and reciprocal of amplitude characteristic compared to that of the secondary plant FRFs, which validates the derivation of Eqs. (2) and (3). However, these derived inverted plants cannot be directly applied in practice since the output of the controller will be amplified to a very large level at certain angular positions where the actuation orientation of the PBRIAs is approximately perpendicular to that of the disturbance force (i.e. between 20° and 40° in Figure 6 (a), and between 75° and 100°, between 285° and 310° in Figure 6 (a)), causing saturation (and as a result also stability) problems. In order to overcome these problems, the

inverted FRFs are modified in a way that the amplitude around these problematic angular positions is attenuated to be comparable to that of adjacent ones, as shown in the graphs in the yellow line.

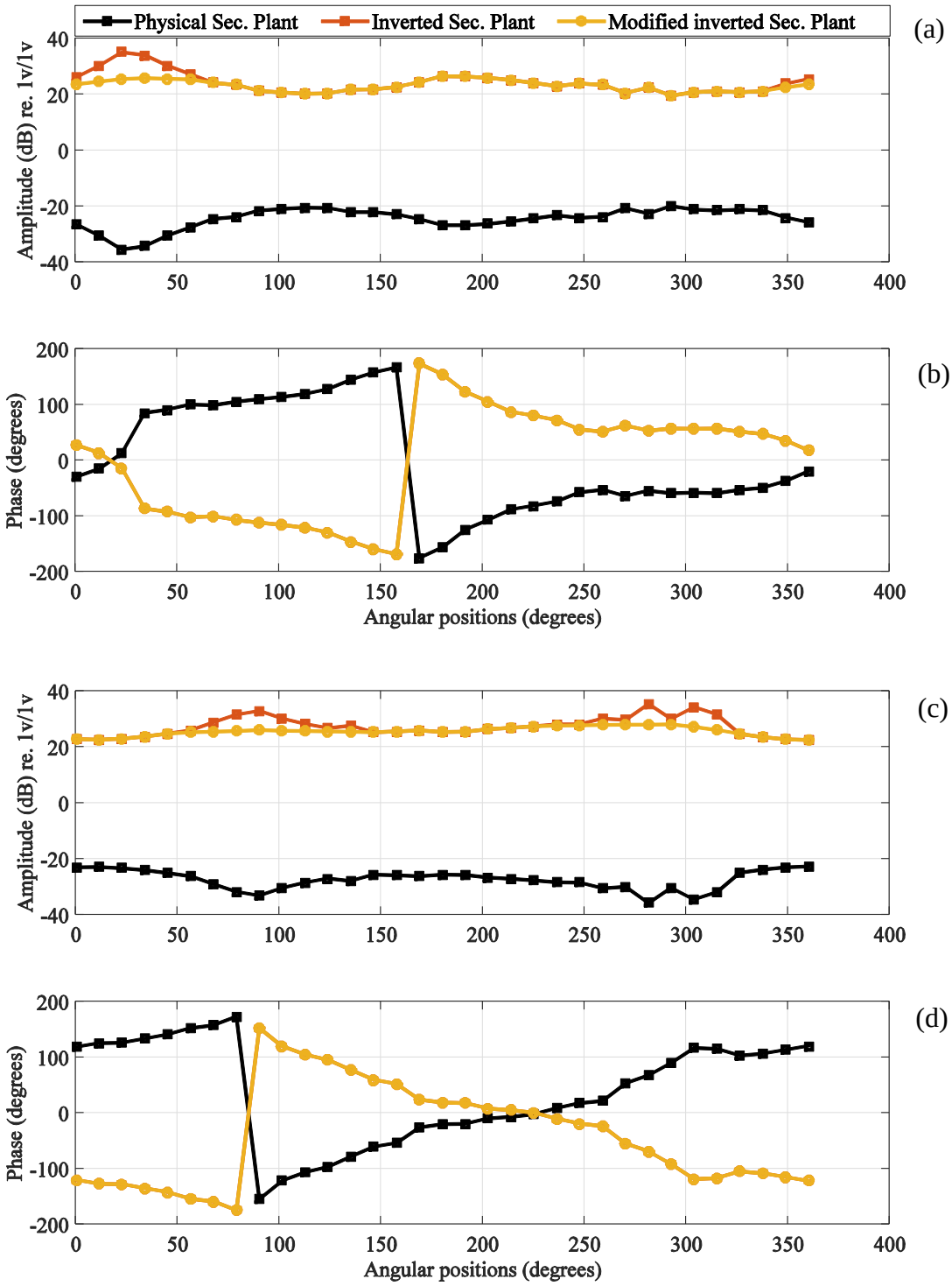

Figure 6: Frequency response functions of the secondary plants at the 32 angular positions: (a) and (b), the amplitude and the phase of the FRFs between the voltage to the PBRIA 1 and the horizontal plate vibration; (c) and (d), the amplitude and the phase of the FRFs between the voltage to the PBRIA 2 and the horizontal plate vibration.

Using these modified inverted secondary plant models, the performance of the developed controller is evaluated over a selected range of operating rotation speeds in the following subsections. The aim is twofold: (i) to demonstrate the feasibility of the proposed ASAC control approach for suppressing structure born noise of gearbox systems, and (ii) to experimentally evaluate the potential and limitations of the proposed control approach at different rpms.

4.2 Rotating tests

In this subsection, experiments are carried out with the shaft rotating at 60, 120 and 180 rpm. The controller filter coefficients are updated using the LMS algorithm. The convergence rate μ is set to 0.003 and the leaky factor β is set to 0.9996. This introduces some penalty on the used power, which is essential in this case for the current SIMO control case where we have two actuators that can suppress the one error signal in multiple manners. By including this penalty, unreasonable values of control effort are prevented. Additional benefits are that this reduces cross-talk between the driving signals, and reduces the risk of instability.

Figure 7(a) shows the measured plate vibrations at the rotating speed of 60 rpm, 120 rpm and 180 rpm (from top to bottom), first with the developed controller deactivated, then activated and afterwards again deactivated. A substantial reduction is obtained for each rpm case when the controller is switched on. However the residue level moderately increases with an increase of the rotation speed. In order to further analyze these results, the achieved reductions are plotted as a function of the rotational angle of the shaft. To do so, the time domain signals of the first two segments (deactivated and activated) are synchronized with the rotation speed signal measured by the encoder, and the reductions are calculated in an interval of 10°. The resultant reductions are shown in the angular domain in Figure 7 (b), where the average reductions during the different revolutions are represented by the dot-line and the variations by the error bars. As shown, the trend of the averaged reductions also indicates that the control effectiveness degrades as the rotation speed increases.

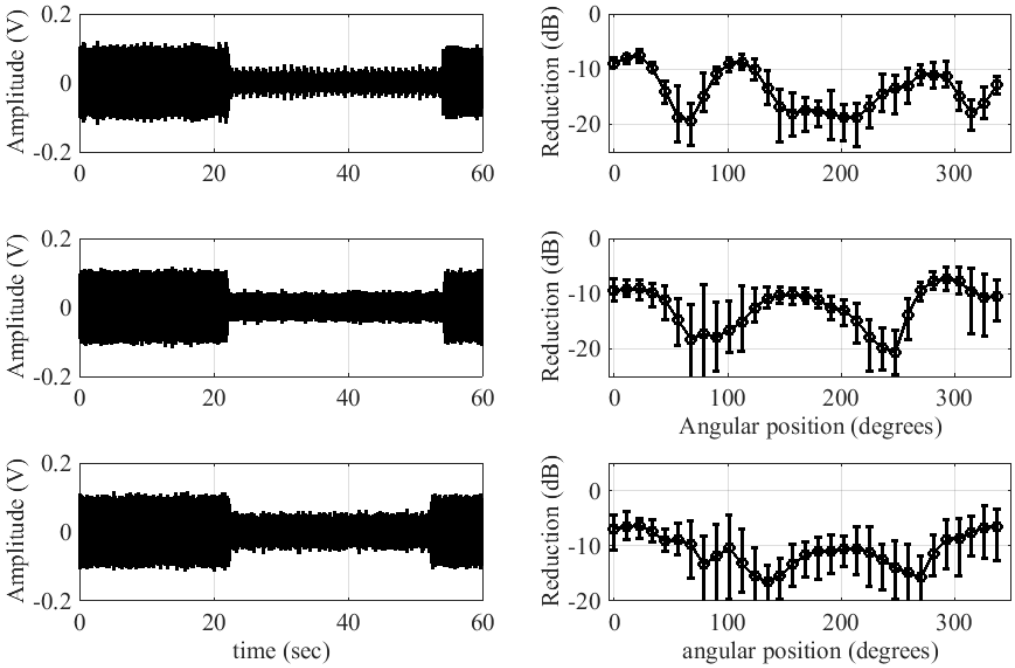

Figure 7: (a) The effect of the pre-learned controller on the plate acceleration when the shaft rotates at, from top to bottom, 60 rpm, 120 rpm and 180 rpm in the time domain; (b) The resultant reductions in the angular domain

The results are then examined in the frequency domain, where the first two segments of the time domain signals in each case are projected into the frequency domain, as shown in Figure 8 (a). The achieved reductions are presented in Figure 8 (b), evaluated at the disturbance frequency itself and three pairs of rotation speed harmonics. It can be seen that a reduction of approximately 15 dB is obtained at the exciting frequency, independent of the rotation speed. However, the reduction at the adjacent harmonics depends on the rotation speed. For example, the reductions at the first rotation speed harmonic decrease with an increase of rpm. The observed degradation of the control effectiveness in Figure 7 can for a large part be explained by the increase of this and some other harmonics. In order to improve the performance, the dynamics of the neighboring rotation speed harmonics should be taken into account and actively suppressed as well. This would then also require increasing the length of the control filter correspondingly, or adding a second LMS controller in parallel, so that each operates at a single frequency. Another reason for the reduced performance with increasing the shaft speed can be found in the non-perfect inclusion of the secondary plants, due to (i) using a linear FIR approximation for a nonlinear behavior, and (ii) ignoring any effects of the rotating speed by forming the overall model by interpolating models identified at fixed angles.

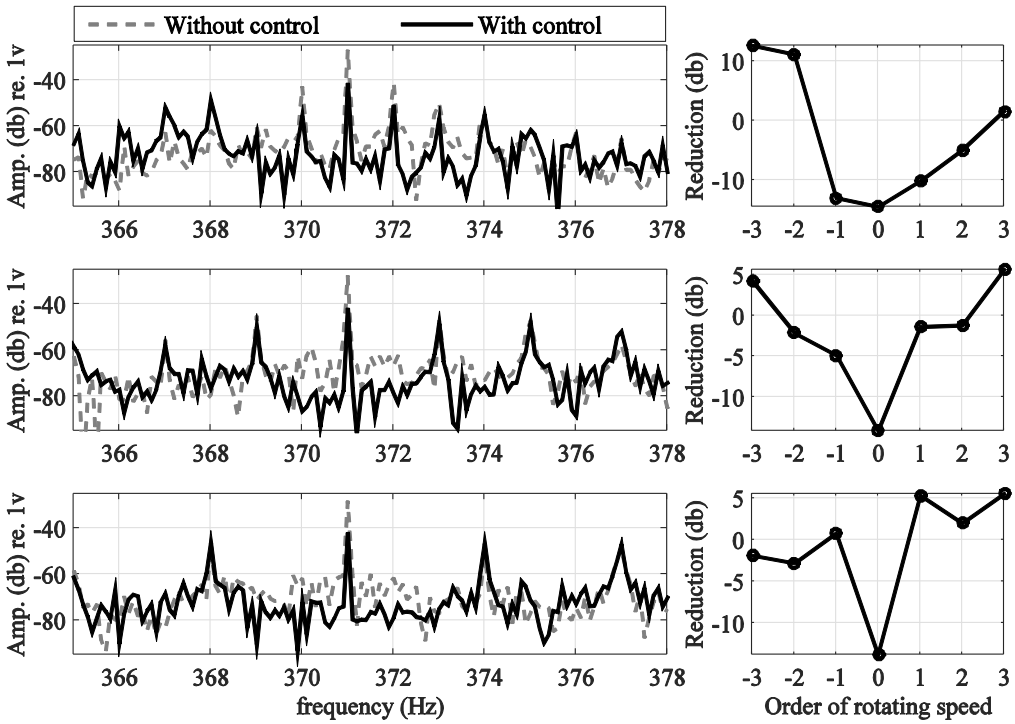

Figure 8: (a) Comparison of the plate vibrations in the frequency domain, without control and with control when the shaft rotates at, from top to bottom, 60 rpm, 120 rpm and 180 rpm; (b) the resultant reductions at the disturbance frequency itself and three pairs of adjacent harmonics.

In the following analysis, the performance of the presented control approach is compared to that of the standard FxLMS controller. The SIMO control scheme of the standard FxLMS controller for the considered case is shown in Figure 9, which can be found in more detail in [26]. Note that the secondary plant models are now placed between the reference signal and the input of the controller, so that the optimal controller coefficients for cancelling the disturbance will be dependent on the angular position, and will have to be adapted over the course of a revolution. When the shaft spins faster, there will be less time for the controller to update their coefficients to the expected ones for the upcoming angular positions.

Figure 10 (a) compares the time of history of the plate vibrations using the two controllers and Figure 10 (b) plots the resultant reductions in the angular domain. As shown, the control effectiveness between the two controllers is comparable at 60 rpm, while the benefit of using the proposed algorithm starts to be more pronounced at higher rpms. These experimental observations imply that the proposed algorithm can outperform its standard FxLMS controller counterpart at relatively higher rotation speeds, caused by the fact that its convergence rate is not much affected by the rotation speed.

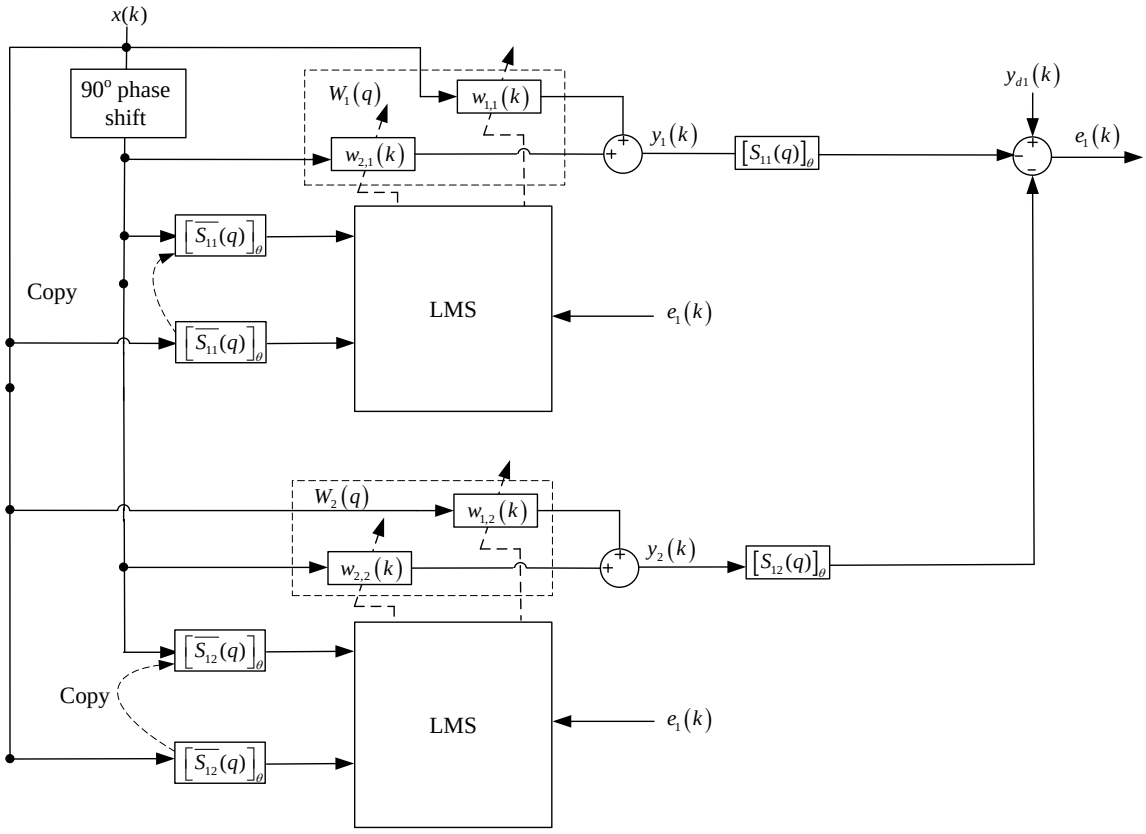

Figure 9: The flowchart of the SIMO form of the FxLMS algorithm utilising a pair of orthogonal harmonic reference signals

5 CONCLUSIONS

This paper discusses a novel control concept for suppressing gear whine noise, which is to use PBRIAs that rotate together with the machinery to actively control the effects of disturbance forces transmitted to the structure housing. A feedforward control strategy similar to the FxLMS control algorithm is proposed to generate the appropriate actuation signals, which aims to limit the influence of the secondary plant variation to the control performance. In order to apply the proposed algorithm for the control situation in this paper, the inverse of a 2nd order FIR filter and an interpolation of FIR filters are utilized. This control approach has been validated on an experimental test bed, where a standard FxLMS SIMO controller is also implemented as a benchmark. Comparing the control performance of the two controllers, it can be seen that the variation of the secondary plant on the control effectiveness is lower if the proposed control scheme is used. Consequently, a reduction of approximately 15 dB in the plate vibrations can be achieved at the disturbance frequency itself, independent of the tested rpms, with the resulting reduction of acoustic noise in the same order of magnitude. However, the overall resultant vibration reductions degrade as the rpm increases, because the proposed control algorithm only aims to cancel the disturbance at a signal frequency, while the response at the uncontrolled rotation speed harmonics increases at higher rpms. Therefore, future studies will aim at improving the performance of the active vibration control approach for higher rotating speeds, as well as gaining a better understanding of the limitations of the followed approach.

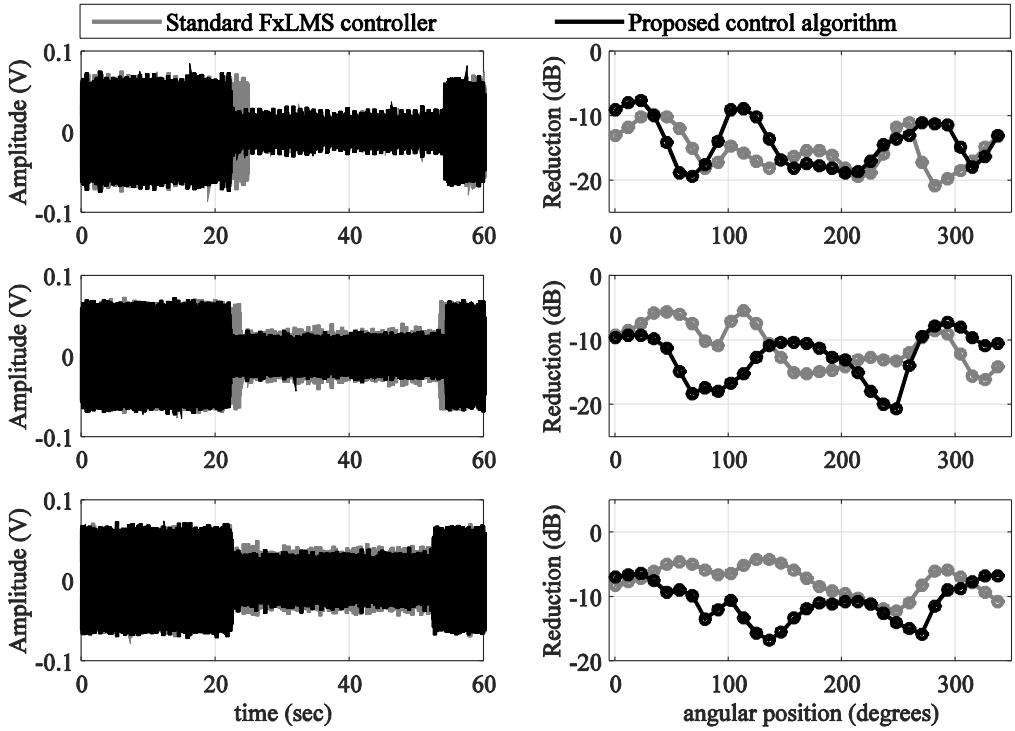

(a) (b)

Figure 10: (a) The control performance comparison of the two controllers in the plate acceleration when the shaft rotates at, from top to bottom, 60 rpm, 120 rpm and 180 rpm in the time domain; (b) Comparison of the resultant reductions in the angular domain.

REFERENCES

[1] P.A. Nelson, S.J. Elliott, Active control of Sound, Academic Press, New York, 1992
[2] S.M. Kuo, D.R. Morgan, Active Noise Control Systems: Algorithms and DSP Implementation, Wiley, New York, 1996.
[3] S.J. Elliott, C.C. Boucher and P.A. Nelson, The behaviour of a multiple channel active control system, IEEE transactions on Signal Processing (1992), Vol. 40(5), 1041-1052.
[4] S. J. Elliott, P. A. Nelson, I. M. Stothers. And C. C. Boucher, Inflight experiments on the active control of propeller-induced cabin noise, Journal of Sound and Vibration, vol. 140. pp. 219-238, 1990.
[5] W. Dehandschutter, The reduction of structure-borne noise by active control of vibration, PhD thesis, KU Leuven University, Leuven, Belgium (1997).
[6] G. Pinte, Active Control of Repetitive Impact Noise, PhD thesis, KU Leuven University, Leuven, Belgium. (2007).
[7] Den Hartog, J. P., Mechanical Vibrations, McGraw-Hill Book Co., New York, (1934.)
[8] J. B. Hunt, Dynamic Vibration Absorbers, London: Mechanical Engineering Publications Ltd. (1979).
[9] D. J. Inman, Engineering Vibration, Prentice-Hall, New York (1994).
[10] N. Alujevic, I. Tomac and P. Gardonio, Tunable vibration absorber using acceleration and displacement feedback, Journal of Sound and Vibration (2012) 331(12), 2713-2728.
[11] C. Paulitsch, P. Gardonio, S. J. Elliott, P. Sas, and R. Boonen, Design of a Lightweight, Electrodynamic, Inertial Actuator with Integrated Velocity Sensor for Active Vibration Control of a Thin Lightly-Damped Panel. International Conference on Noise and

Vibration Engineering (ISMA), Katholieke Universiteit Leuven, Belgium, 20-23 September 2004.
[12] C. Paulitsch, P. Gardonio, S.J. Elliott, Active vibration control using an inertial actuator with internal damping, Journal of the Acoustical Society of America 119 (2006) 2131–2140.
[13] N. Alujevic, G. Zhao, B. Depraetere, P. Sas, B. Pluymers and W. Desmet, $\mathcal{H}2$ optimal vibration control using inertial actuators and a comparison with tuned mass dampers, Journal of Sound and Vibration (2014), 333(18), 4073-4083.
[14] N. Alujevic, P. Gardonio, and K. D. Frampton, Smart double panel for the sound radiation control: blended velocity feedback. AIAA Journal, vol. 49. No. 6 (2011), pp. 1123-1134.
[15] Z. Qiu, X. Zhang, H. Wu and H. Zhang, Optimal placement and active vibration control for piezoelectric smart flexible cantilever plate, Journal of Sound and Vibration (2007) 301, 521-543.
[16] E. Crawley and J. de Luis, Use of piezoelectric actuators as elements of intelligent structures, AIAA Journal 25 (1987) 1373-1385.
[17] C. R. Fuller, S. J. Elliott and P. A. Nelson, Active control of Vibration, Academic Press, San Diego, CA92101, 1986.
[18] T. J. Sutton, S. J. Elliott, M. J. Brennan, K. H. Heron and D. A. C. Jessop, Active Isolation of Multiple Structural Waves on a Helicopter Gearbox Support Strut, Journal of Sound and Vibration (1997) 205(1), 81-101.
[19] B. Rebbechi, C. Howard and C. Hansen, Active control of gearbox vibration, Proceedings of the Active control of Sound, Vibration conference, Fort Lauderdale, 1999, pp. 295-304.
[20] G. Pinte, S. Devos, B. Stallaert, W. Symens, J. Swevers and P. Sas, A piezo-based bearing for the active structural acoustic control of rotating machinery. Journal of Sound and Vibration, 329 (2010) 1235-1253.
[21] B. Stallaert, Active structural acoustic source control of rotating machinery, PhD thesis, KU Leuven University (2010).
[22] M. H. Chen, M. J. Brennan, Active control of gear vibration using specially configured sensors and actuators, Smart Materials and Structures 9(3) 2000 342-350.
[23] Y.H. Guan, M. Li, T.C. Lim and W.S. Shenpard Jr., Comparative analysis of actuator concepts for active gear pair vibration control, Journal of Sound and Vibration, 269 (1-2) (2004) 273-294.
[24] Y.H. Guan, T.C. Lim and W.S. Shenpard Jr., Experimental study on active vibration control of a gearbox system, Journal of Sound and Vibration, 282 (3-5) (2005) 713-733.
[25] M. Li, T.C. Lim, W.S. Shenpard Jr. Y.H. Guan, Experimental active vibration control of gear mesh harmonics in a power recirculation gearbox system using a piezoelectric stack actuator, Smart Materials and Structures, 14 (5) (2005) 917-927.
[26] G. Zhao, N. Alujevic, B. Depraetere, G. Pinte, J. Swevers, P. Sas. Experimental study on active structural acoustic control of rotating machinery using rotating piezo-based inertial actuators. Journal of Sound and Vibration (2015), DOI: 10.1016/j.jsv.2015.03.013.